This article has been accepted for publication in IEEE Transactions on Power Electronics. This is the author's version which has not been fully edited and content may change prior to final publication. Citation information: DOI 10.1109/TPEL.2023.3239160

GaN-Based Matrix Resonant Power Converter for Domestic Induction Heating

Pablo Guillen, *Student Member, IEEE*, Hector Sarnago, *Senior Member, IEEE*, Oscar Lucia, *Senior Member, IEEE*, and Jose Miguel Burdio, *Senior Member, IEEE*

***Abstract*— Flexible-surface induction cooktops must operate with a variety of induction heating loads with different behavior and power setpoints to be heated simultaneously. In this context, multi-output inverter topologies aim at achieving independent power management while featuring low power-device count and high power density. However, they suffer from limitations when applying classical modulation strategies to ensure soft switching, which is required to reduce transistor losses and achieve efficient operation. In this scenario, wide band-gap devices reduce switching losses, opening a new paradigm in power conversion where soft switching is not mandatory in order to achieve high efficiency. This paper proposes an implementation of a multi-output resonant inverter based on GaN HEMTs and evaluates various modulation strategies in terms of efficiency under different switching modes. The proposed approach is designed and experimentally validated by means of a 2-coil 2000 W prototype implementation.**

***Index Terms*— Home appliances, Induction Heating, Wide Band Gap, Multi-output inverter**

I. Introduction

DOMESTIC induction heating (IH) pursue of flexibility relies on the usage of multi-coil structures to generate optimal temperature profiles in the pot base. As a consequence, the different inductor-pot systems can be considered independent IH-loads with their corresponding electrical equivalent parameters and power setpoints [1-5].

In order to address the multi-load power transmission challenge, multi-output topologies, derived from the full bridge [6-9], half bridge [10-12] and single switch [13], have been developed. These topologies balance complexity, versatility and efficiency depending on the characteristics of the application, e.g. inductor size, inductor number, target material, heating distance, etc.

In [14], a cost-effective and versatile family of multi-output resonant inverters, derived from the half-bridge topology, is described. This letter further develops this idea by proposing a high-efficiency implementation of an array multi-output converter with a column structure able to operate under load mismatch achieving reduced power losses, which eases integration in a flexible induction heating cooktop.

The remainder of this paper is organized as follows. Section II presents the patented multi-output converter family, describes the selected topology, and defines the independent control parameters and operation. Section III describes the prototype implementation. Section IV shows the main experimental results and Section V draws the main conclusions.

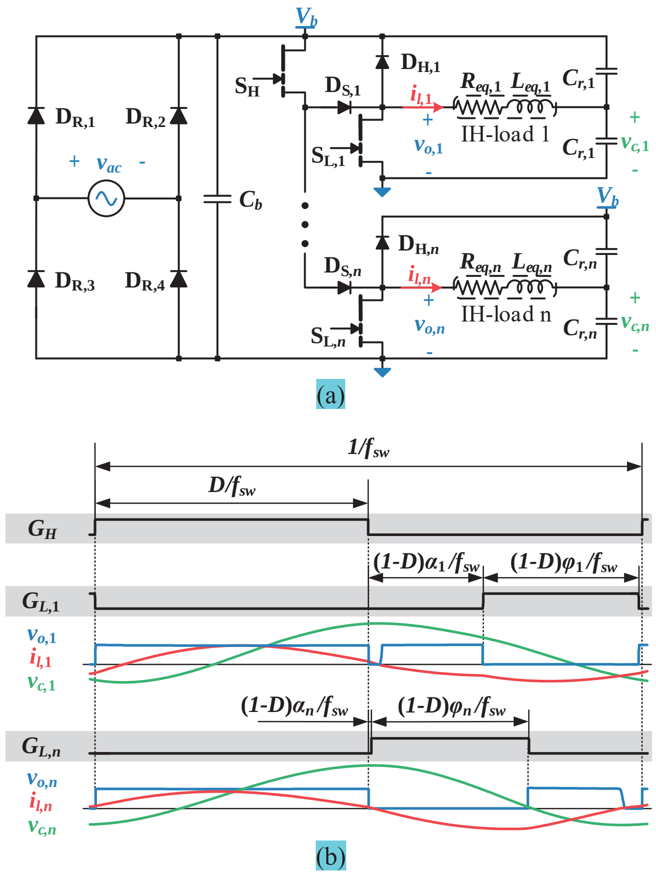

Fig. 1. Array multi-output ZVS resonant converter with column structure (a), and non-complementary pulse delay control modulation parameters and waveforms (b), being α the driving parameter in IH-load 1 and φ the driving one in IH-load n.

This work was partly supported by the Spanish MICINN under Projects AEI PID2019-103939RB-I00, PDC2021-120898-I00, TED2021-129274B-I00, CPP2021-008938, ISCIII PI21/00440, co-funded by EU through FEDER and NextGenerationEU/PRTR programs, by the DGA-FSE, by the MECD under the FPU grant FPU17/01442, and by the BSH Home Appliances Group.

The authors are with the Department of Electronic Engineering and Communications, I3A, Universidad de Zaragoza, 50018 Zaragoza, Spain (e-mail: pguillenm@unizar.es; hsarnago@unizar.es; olucia@unizar.es; burdio@unizar.es).

Color versions of one or more of the figures in this article are available online at http://ieeexplore.ieee.org

This article has been accepted for publication in IEEE Transactions on Power Electronics. This is the author's version which has not been fully edited and content may change prior to final publication. Citation information: DOI 10.1109/TPEL.2023.3239160

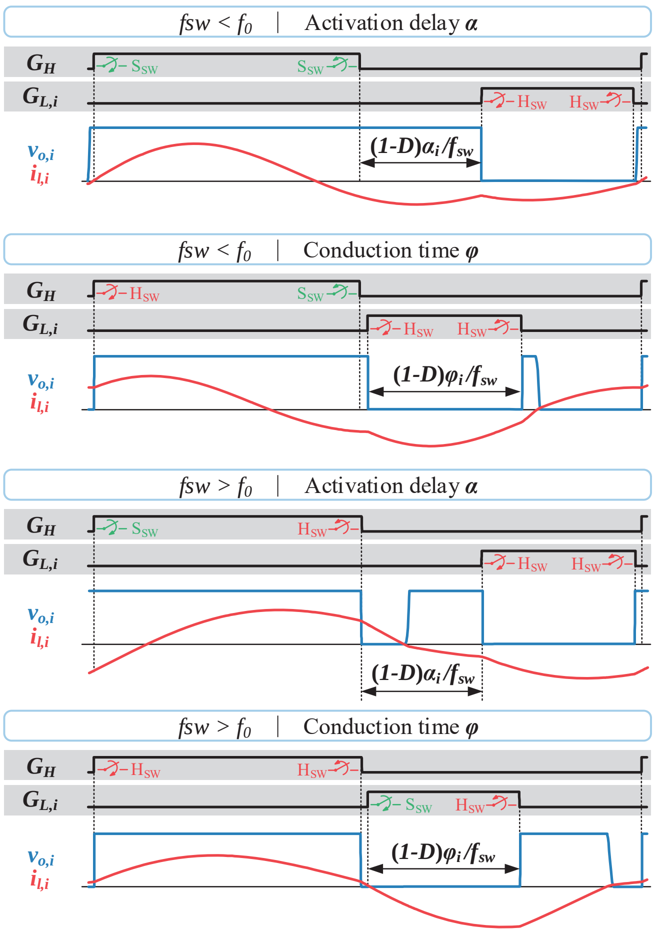

Fig. 2. Load waveforms for nominal power when operating under and over resonant frequency, f_0, and varying a low-side transistor parameter to achieve power control. Additionally, switching sequeces are labeled as hard switching, H_{SW}, and soft switching, S_{SW}.

II. Matrix-Derived Multi-Output Resonant Inverter

The proposed converter family aims to provide multi-output converters with reduced power device count. The matrix implementation is designed for a high number of coils achieving independent load activation [15], but it presents restrictions in power control. Therefore, for a medium number of coils, i.e. 2-6 coil appliances, array topologies are preferred, as they increase the power control flexibility while maintaining a reduced increase of power devices with the number of coils.

The selected topology (Fig. 1 (a)) is an array inverter with a column structure that presents a common high-side transistor, S_H, and up to n branches that present each, $i \in [1, n]$, a series diode, $D_{S,i}$, high-side diode, $D_{H,i}$, and low-side transistor, $S_{L,i}$, with its intrinsic body diode that can be referred as $D_{L,i}$. Each IH-load is represented by their equivalent resistance, $R_{eq,i}$, and inductance, $L_{eq,i}$, and the resonant tank is completed by the split resonant capacitor, C_r.

The independent control parameters to establish the transferred power to a load are the activation delay, t_d, and active time, t_{on}, of each transistor [16], which, considering steady state and regarding the common high-side transistor, can be expressed as:

$$t_{d,H} = 0 \qquad t_{on,H} = D/f_{sw}$$
$$t_{d,L,i} = (1-D)\alpha_i / f_{sw} \qquad t_{on,L,i} = (1-D)\varphi_i / f_{sw} \tag{1}$$

Being f_{sw} the switching frequency and D the duty cycle. α_i is the low-side transistor activation delay, and φ_i the low-side transistor active time, defined guaranteeing $\alpha_i + \varphi_i \leq 1$. These resulting parameters are presented in Fig. 1 (b).

Thus, the behavior of each of the branches can be described with the solution of the following algebraic differential equations, that show the dependence of the applied voltage, $v_{o,i}$, with the active transistor or the load current, $i_{l,i}$, path when no transistor is active:

$$v_{o,i} = V_b\left(G_H + (1-G_H)(1-G_{L,i})\left(1-\frac{1}{1+e^{-\lambda_D i_{l,i}}}\right)\right),$$
$$\frac{di_{l,i}}{dt} = \frac{1}{L_{eq,i}}\left(v_{o,i} - R_{eq,i} i_{l,i} - v_{c,i}\right), \tag{2}$$
$$\frac{dv_{c,i}}{dt} = \frac{1}{C_r} i_{l,i}.$$

Where V_b is the bus voltage, $v_{c,i}$ is the load capacitor voltage, and λ_D is the parameter that allow the modelling of the voltage change across the antiparallel diodes as a consequence of the change in the current direction. Additionally, G_H and $G_{L,i}$ are the normalized gate signals, that can be described in a continuous form [17] as:

$$G_H = \frac{1}{\left(1+e^{\lambda_S\left(-\sin(2\pi f_{sw}t - \pi D + \pi/2) + \sin(\pi/2 - \pi D)\right)}\right)},$$
$$G_{L,i} = \frac{1}{\left(1+e^{\lambda_S\left(-\sin\left(2\pi f_{sw}t - 2\pi\left(D+(1-D)(\alpha_i+\varphi_i/2)\right)+\pi/2\right)+\sin\left(\pi/2-\pi(1-D)\varphi_i\right)\right)}\right)}. \tag{3}$$

Being λ_S the parameter that allow the modelling of the voltage change due to the switching of the transistors. Therefore, to achieve the same output power, $P_{o,i}$, several

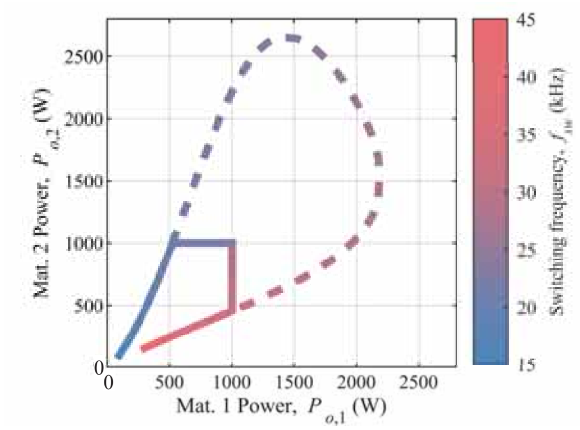

Fig. 3. Maximum simultaneous transmissible power for two different pot materials in the complete frequency range. Additionally, the curve for nominal power is also depicted.

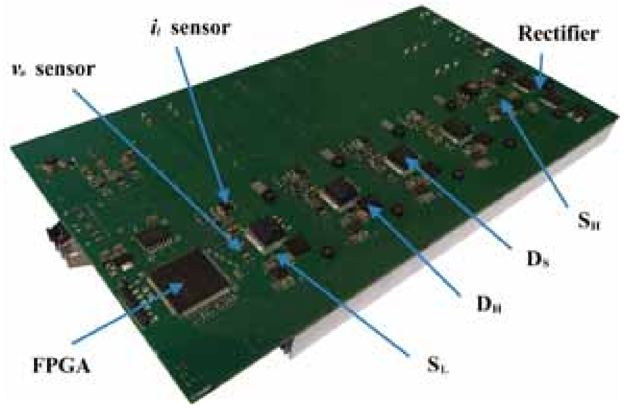

Fig. 4. Propossed converter prototype.

alternatives are possible, leading to different waveforms and switching sequences as it can be seen in Fig. 2. There, the operation under and above the resonant frequency, i.e. capacitive and inductive load behavior, modifying a low-side transistor parameter is presented.

The low-side transistor modulation result in independent power control. Fig. 3 shows the maximum simultaneous power transmission to two different pot materials as a function of the switching frequency. It is possible to reduce the transmitted power to each of them by increasing activation delay, α_i, or reducing conduction time, φ_i. Additionally, power curves show a wide frequency range where low-side transistor parameters allow to operate at nominal power, i.e. 1000 W, solving problems such as IH-loads equivalent parameters mismatch.

III. Proposed Prototype

A prototype considering wide frequency range operation and oval-shaped coils has been designed. Considering typical commercial pots, the following electrical equivalent parameters are obtained $L_{eq,i}$ ϵ [60 µH, 117 µH], $Q = 2\pi f_{sw} L_{eq,i}/R_{eq,i}$ ϵ [2.15, 4.59], and C_r = 400 nF is selected to operate in the desired frequency range. With these parameters, a prototype featuring WBG devices has been designed. This proposal aims for reducing switching losses even under hard-switching conditions achieving a high efficiency implementation.

In order to do so, GaN HEMTs are selected as the main power devices. Due to the additive current through the high-side transistor, GS66516T with an on resistance of 25 mΩ (T_j = 25 ºC) is chosen. GS66508T, that presents a resistance of 50 mΩ, is used for the low-side transistors resulting in a cost-effective implementation without critical components, i.e. devices that present higher temperatures in operation. In order to improve heat management, the transistors are top cooled and placed directly on the heatsink.

The driving circuit is selected to provide +6 V and -4 V voltages to improve noise immunity due to low threshold voltage of the GaN HEMTs. Both high-side and low-side circuits use the driver UCC5350, taking advantage of its isolation for the case of the high-side transistor.

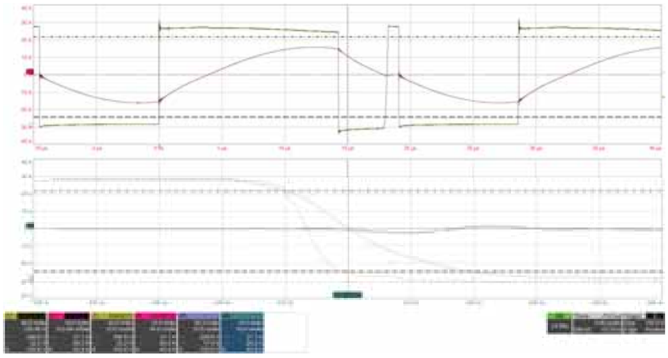

Fig. 5. Main operation waveforms and detail of load voltage change during low-side transistor hard-switching turn-on sequence. On the general plot pane: output voltage, $v_{o,i}$, (40 V/div, yellow) and inductor current, $i_{l,i}$, (10 A/div, pink). Time axis: 5 µs/div. On the zoomed plot pane: GaN prototype output voltage, $v_{o,i}$, (40 V/div, yellow), GaN prototype inductor current, $i_{l,i}$, (10 A/div, pink), Si prototype output voltage, $v_{o,i}$, (40 V/div, purple), and Si prototype inductor current, $i_{l,i}$, (10 A/div, blue). Time axis: 10 ns/div.

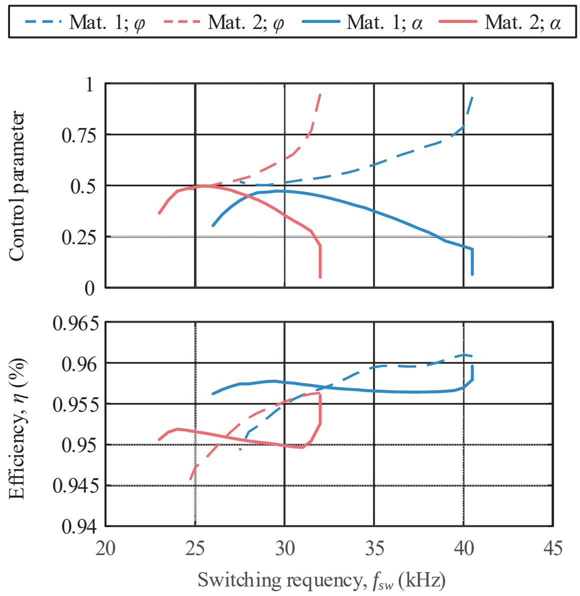

Fig. 6. Efficiency curves for nominal power, 1000 W, transmission at different operation frequency, modifying low-side transistor α_i or φ_i parameters.

Depending on the different requirements of each diode, a different technology has been selected. Thus, schottky SiC diodes are used as the branch series diode, STPSC20065-Y, and branch antiparallel diode, STPSC6H065DLF, due to the low reverse recovery. Standard rectifier diodes, SE20DLJ, are chosen for the discrete mains rectifier. This selection is made based upon both the electrical characteristics and the packaging in order to get a proper thermal management. Thus, D2PAK packaging is combined with metal inlay cooling, and thermal vias are placed underneath the antiparallel diode [18].

The converter includes both load current and voltage measurements and the overall control is performed by means

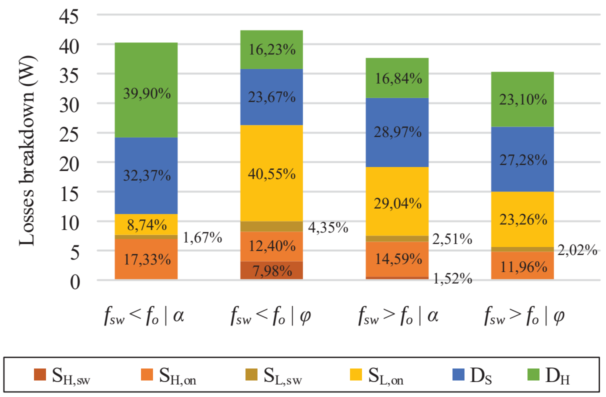

Fig. 7. Breakdown of the power loss contribution of the inverter, depending on the switching frequency, f_{sw}, and the modulation strategy used.

of a FPGA whose programed blocks include the PWM modulator, IH load power and current measurement, mains zero crossing detection, and communication with the PC.

III. Experimental Results

In order to validate the prototype correct operation and WBG fast switching, Fig. 5 shows the load voltage and current when operating with a IH load in the inductive region and controlled by means of the α modulation parameter. Moreover, the low-side transistor hard switching turn-on sequence is zoomed and compared with the one of a silicon transistor in an equivalent implementation, showing reduced switching times. As a consequence, switching losses are minimized, leading to a reduction in the power losses of the converter of more than 10%.

The efficiency results for nominal power transmission are presented in Fig. 6 as a function of the switching frequency. The results are measured with the YOKOGAWA PZ4000 power analyzer and are corelated to the low-side transistor parameter fluctuation necessary to achieve the desired power. In Fig. 7, a power loss breakdown based on the device conduction and switching parameters is shown. There, the dependencies with the switching frequency and modulation strategies can be seen, highlighting the minimal contribution of the switching losses in most of the cases.

Moreover, in Fig. 6 it can be seen that the frequency range of the different loads presents an overlap, ensuring simultaneous multi-load operation up to nominal power. The variation on the required activation delay, α, or conduction time, φ, depending on the switching frequency, f_{sw}, can be seen in Fig. 8. There, control versatility of the multi-coil system, which ensures independent power control while avoiding acoustic noise is shown.

Additionally, in order to generalize the multi-load operation of the converter, Fig. 9 depicts nominal power transmission to three IH load. In this case IH-load 2 and 3 present the same material but a different low-side transistor modulation parameter control for each one. This shows the independence in the parameter setting and therefore the control of the transmitted power to each of the loads provided that f_{sw} remains in the range where nominal power is ensured for all

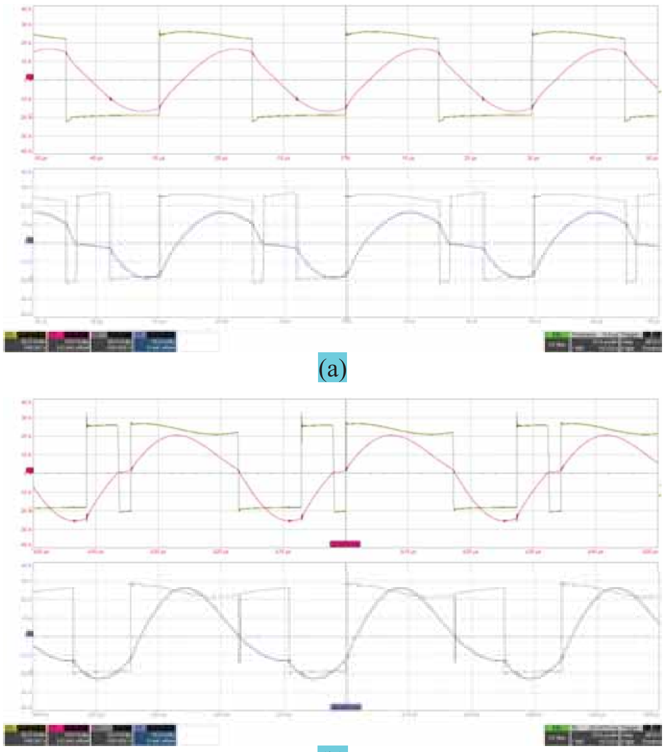

(a)

(b)

Fig. 8. Main waveforms of multi-load operation with nominal power transmission to two different loads operating in the maximum efficiency point at f_{sw} = 33.3 kHz (a) and f_{sw} = 29 kHz (b). In each oscilloscope screen capture, from top to bottom: IH-load 1 output voltage, $v_{o,1}$, (50 V/div, yellow), IH-load 1 inductor current, $i_{l,1}$, (10 A/div, pink), IH-load 2 output voltage, $v_{o,2}$, (50 V/div, grey), IH-load 2 inductor current, $i_{l,2}$, (10 A/div, blue). Time axis: 10 µs/div.

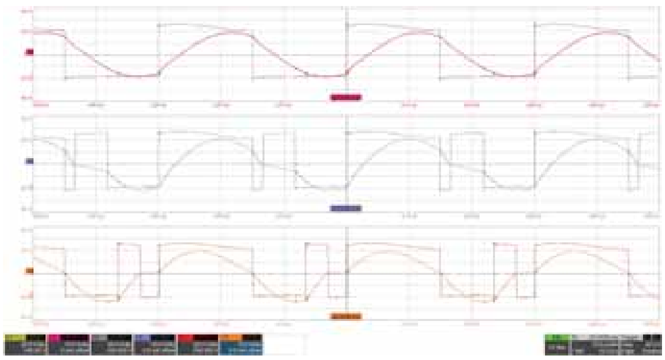

Fig. 9. Main waveforms of multi-load operation with nominal power transmission to three different loads using NC-PDM and NC-PWM modulation strategies simultaneously. From top to bottom: IH-load 1 output voltage, $v_{o,1}$, (50 V/div, yellow), IH-load 1 inductor current, $i_{l,1}$, (10 A/div, pink), IH-load 2 output voltage, $v_{o,2}$, (50 V/div, grey), IH-load 2 inductor current, $i_{l,2}$, (10 A/div, blue), IH-load 3 output voltage, $v_{o,3}$, (50 V/div, red), IH-load 3 inductor current, $i_{l,3}$, (10 A/div, orange). Time axis: 10 µs/div.

TABLE I
PERFORMANCE COMPARISON OF THE PROPOSED CONVERTER

REFERENCE	IH LOADS	FREQUENCY RANGE (KHZ)	EFFICIENCY (%)	SIMULTANEOUS ACTIVATION	INDEPENDENT POWER CONTROL	TRANSISTORS	DIODES
[19]	n	30 - 150	92%	YES	IF $f_i << f_{i+1}$	$2n$	0
[20]	2	50 - 100	97%	NO	YES	4	0
[7]	n	400 - 700	99%	YES	YES	$2 + 2n$	2
[8]	2	30	91%	NO	YES	4 + 4	0
[15]	n	20 - 100	98%	YES	NO	$\sqrt{n}$	$2n$
[12]	3	30 - 150	96%	NO	IF $f_i << f_{i+1}$	3	0
[21]	3	20 - 400	92%	YES	IF $f_i << f_{i+1}$	8	0
PROPOSED	n	25 - 40	96%	YES	YES	$1 + n$	$2n$

active loads. Moreover, the increase on the number of loads should consider the additive currents through the high-side transistor, which is limited by the maximum power of the converter, that might be lower than the sum of the loads.

Based on the experimental results, it is possible to compare the proposed converter with similar multi-output ones in the literature. This comparison is presented in Table I, where the proposal stands out for the versatility in the power control, allowing simultaneous and independent power transmission. This feature, in addition to the reduced number of controlled power devices, being most of them ground-referenced, and overall high efficiency make the proposal a unique solution for driving multi-coil structures with highly-variable IH loads.

V. CONCLUSION

High-efficiency multi-output converters are a key enabling technology for the widespread of flexible surface induction heating cooktops. Due to the application characteristics, complex modulation strategies appear, requiring an additional effort in the topology design, ensuring reduced power losses regardless the nature of the switching sequence.

In this paper a WBG implementation of a multi-output converter is developed to provide accurate power control and highly efficient operation even with loads with different equivalent parameters. This has been experimentally verified and switching sequences have been compared with similar implementations with silicon devices.

The prototype presents a peak efficiency over 96% for nominal power operation. Additionally, it is shown that high efficiency operation is achieved for a wide frequency range, allowing a high versatility in the simultaneous power transmission to different loads.

REFERENCES

[1] H. N. Pham *et al.*, "Dynamic Analysis and Control for Resonant Currents in a Zone-Control Induction Heating System," *IEEE Transactions on Power Electronics,* vol. 28, no. 3, pp. 1297-1307, 2013.

[2] F. Forest *et al.*, "Principle of a multi-load/single converter system for low power induction heating," *IEEE Transactions on Industrial Electronics,* vol. 15, no. 2, pp. 223-230, March 2000.

[3] O. Lucía *et al.*, "Induction heating appliances: Towards more flexible cooking surfaces," *IEEE Industrial Electronics Magazine,* vol. 7, no. 3, pp. 35-47, September 2013.

[4] J. Acero *et al.*, "Mutual Impedance of Small Ring-Type Coils for Multiwinding Induction Heating Appliances," *IEEE Transactions on Power Electronics,* vol. 28, no. 2, pp. 1025-1035, 2013.

[5] E. Jang *et al.*, "Analysis and Design of Flexible-Surface Induction-Heating Cooktop With GaN-HEMT-Based Multiple Inverter System," *IEEE Transactions on Power Electronics,* vol. 37, no. 10, pp. 12865-12876, 2022.

[6] S. Zenitani *et al.*, "A charge boost type multi output full bride high frequency soft switching inverter for IH cooking appliance," in *Proceedings of 14th International Power Electronics and Motion Control Conference EPE-PEMC 2010*, 2010, pp. T2-127-T2-133.

[7] H. Sarnago *et al.*, "Design and Implementation of a High-Efficiency Multiple-Output Resonant Converter for Induction Heating Applications Featuring Wide Bandgap Devices," *IEEE Transactions on Power Electronics,* vol. 29, no. 5, pp. 2539-2549, 2014.

[8] V. B. Devara *et al.*, "Capacitor-sharing two-output series-resonant inverter for induction cooking application," *IET Power Electronics,* vol. 9, no. 11, pp. 2240-2248, 2016.

[9] S. K. Papani *et al.*, "Dual frequency inverter configuration for multiple-load induction cooking application," vol. 8, no. 4, pp. 591-601, 2015.

[10] Y.-C. Jung, "Dual half bridge series resonant inverter for induction heating appliance with two loads," *Electronics Letters,* vol. 35, no. 16, pp. 1345-1346, May 1999.

[11] F. Forest *et al.*, "Frequency-synchronized resonant converters for the Supply of multiwindings coils in induction cooking appliances," *IEEE Transactions on Industrial Electronics,* vol. 54, no. 1, pp. 441-452, February 2007.

[12] B. Salvi *et al.*, "A Three Switch Resonant Inverter for Multiple Load Induction Heating Applications," *IEEE Transactions on Power Electronics,* vol. 37, no. 10, pp. 12108-12117, 2022.

[13] J. M. Leisten *et al.*, "Single ended resonant power supply for induction heating," *Electronics Letters,* vol. 26, no. 12, pp. 814-816, 1990.

[14] J. Burdío *et al.*, "DOMESTIC APPLIANCE," Patent Appl. US11153940B2, 2021.

[15] H. Sarnago *et al.*, "Multiple-Output ZVS Resonant Inverter Architecture for Flexible Induction Heating Appliances," *IEEE Access,* vol. 7, pp. 157046-157056, 2019.

[16] I. Millan *et al.*, "Improved Performance of Half-Bridge Series Resonant Inverter for Induction Heating with Discontinuous Mode Control," in *APEC 07 - Twenty-Second Annual IEEE Applied Power Electronics Conference and Exposition*, 2007, pp. 1293-1298.

[17] Y. Lu *et al.*, "Sigmoid Function Model for a PFM Power Electronic Converter," *IEEE Transactions on Power Electronics,* vol. 35, no. 4, pp. 4233-4241, 2020.

[18] E. Laloya *et al.*, "Heat Management in Power Converters: From State of the Art to Future Ultrahigh Efficiency Systems," *IEEE Transactions on Power Electronics,* vol. 31, no. 11, pp. 7896-7908, 2016.

[19] S. K. Papani *et al.*, "Dual frequency inverter configuration for multiple-load induction cooking application," *IET Power Electronics,* vol. 8, no. 4, pp. 591-601, 2015.

[20] H. Sarnago *et al.*, "Dual-Output Boost Resonant Full-Bridge Topology and its Modulation Strategies for High Performance Induction Heating Applications," *IEEE Transactions on Industrial Electronics,* vol. PP, no. 99, pp. 1-1, 2016.

[21] S. Khatroth *et al.*, "Cascaded full-bridge resonant inverter configuration for different material vessel induction cooking," vol. 13, no. 19, pp. 4428-4438, 2020.